Available online at www.sciencedirect.com
SCIENCE DIRECT®
Journal of Non-Crystalline Solids 336 (2004) 84–95
JOURNAL OF NON-CRYSTALLINE SOLIDS
www.elsevier.com/locate/jnoncrysol

Bubble transport in three-dimensional laminar gravity-driven flow – numerical results

Laurent Pilon [a,*], Raymond Viskanta [b]

[a] Department of Mechanical and Aerospace Engineering, University of California, Room 46-147C, Los Angeles, CA 900095-1597, USA
[b] Heat Transfer Laboratory, School of Mechanical Engineering, Purdue University, West Lafayette, IN 47907, USA

Received 15 October 2003

Abstract

This paper is the second part of a study on bubble transport, growth and shrinkage in three-dimensional gravity driven flow. Sample calculations with applications to glass melting furnaces are presented. First, a consistent set of thermophysical properties of the most common composition ($74SiO_2$–$16Na_2O$–10CaO (mol%)) of soda-lime silicate glass or similar compositions over the temperature range of 1000–2000 K is reported. The population balance equation is solved for the bubble density function using the backward method of characteristics. The zeroth to third order moments, i.e., number of bubbles, average radius, molar gas fraction, interfacial area, and void fraction are computed by numerical integration. Results for both transient and steady state operations are presented and analysed. Two cases are considered (1) bubbles containing only CO_2 and (2) bubbles containing a diffusing gas (O_2) and a non-diffusing gas (CO_2). The feasibility of such complex calculation is demonstrated and is in qualitative agreement with reported results.

1. Introduction

The first part of the study [1] presents a comprehensive model of bubble growth, shrinkage, and transport in three-dimensional gravity driven flow. Previous studies computed the dissolved gas concentration in the melt by neglecting the source term due to the diffusion of gases in and out of the bubbles [2–6]. This simplification implies that the dissolved gas concentrations and the number of bubbles in discretized groups can be computed consecutively and independently. In the present study, these parameters are intimately coupled, i.e., $C_{\infty,i}$, r, γ_i, and f_1 are computed iteratively until converged solutions for all the variables are obtained. Considering refining reactions that are complete and irreversible enables one to compute the refining agent concentration $[M^{k+}]$ independently.

The input parameters governing the problem are: (1) the thermophysical properties of the molten glass, (2) the physicochemical properties of gases dissolved in the molten glass, (3) the refining reactions characteristics, (4) the partial pressure of gases at the combustion space/glassmelt or foam interfaces, and (5) the three-dimensional flow and temperature fields of the molten glass. Two sample calculations are presented and discussed in detail for the following physical situations: (1) bubbles contain only CO_2 that diffuse out of the bubbles, and (2) bubbles containing both CO_2 and O_2 but with only O_2 diffusing in and out of the bubbles.

The main goal of this paper is to demonstrate the feasibility of the calculations by presenting sample results and trends observed in the two-phase flow. Consequently, some simplifications in the model formulation have been made to make the calculations more economical. These include neglecting the effect of bubbles on the liquid flow and thermal structures and assuming that the bubble velocity is the same as that of the glassmelt except in the vertical direction where buoyancy is accounted for. These simplifications are justified by the fact that bubbles and the void fraction are small and by the inability to validate the numerical results at present due to the lack of experimental data. The study also aims at assessing the effect of the gas diffusion in and out

* Corresponding author. Tel.: +1-310 206 5598; fax: +1-310 206 4830.
E-mail address: pilon@seas.ucla.edu (L. Pilon).

0022-3093/$ - see front matter © 2004 Elsevier B.V. All rights reserved.
doi:10.1016/j.jnoncrysol.2004.01.007

Nomenclature

A	parameters of the initial bubble size distribution
A_i	liquid/gas interfacial area concentration
B	parameters of the initial bubble size distribution
D	diffusion coefficient
f_1	bubble density function
f_v	volumetric gas fraction
g	specific gravity
M	molecular mass
N	total number of bubbles per unit volume of glassmelt
p_0	atmospheric pressure
p	pressure
r	bubble radius
r_0	initial bubble radius
r_{min}	minimum bubble radius
$\dot{r}$	rate of change of bubble radius
R	universal gas constant = 8.314 J/mol K
S	solubility of the gas species in the molten glass
T	temperature
t	time
W	glass tank width (see Fig. 1)
w_r	vertical upward velocity of the bubble relative to the glassmelt
$\vec{x}$	spatial or external coordinates
x	longitudinal location (see Fig. 1)
x	spanwise location (see Fig. 1)
z	local depth within the glassmelt (see Fig. 1)

Greek symbols

α	parameter
ϵ_1, ϵ_2	arbitrarily small constants for convergence criteria
η	parameters of the initial bubble size distribution
γ	gas molar fraction in the bubbles
σ	surface tension
ρ	density
μ	kinematic viscosity

Subscripts

b	refers to a single bubble
batch	refers to the glassmelt/batch interface
CO_2	refers to the carbon dioxide
i	index of the gas species
I, J, K	refers to indices of the scalar nodes of the staggered grid
O_2	refers to the oxygen
∞	refers to the bulk of the glassmelt

Notation

$\overline{X}$	average value of variable X with respect to bubble radius

of the bubbles on the concentration of dissolved gases in the glassmelt and neglected in previous studies [2–7].

2. Physicochemical properties

The thermophysical properties are important input parameters and their appropriate specification is a major concern in modeling glass melting furnaces and bubble behavior [8,9]. Up to now, no reported simulation of glass melting furnaces has used a consistent set of thermophysical properties for a given glass composition. The assessment of the bubble transport and foam formation models depends strongly on the accuracy of the molten glass thermophysical properties (e.g., viscosity, density, surface tension, thermal diffusivity, and expansion coefficient), the refining reaction characteristics as well as the diffusion coefficient, and the solubility of each gas dissolved in the molten glass. These thermophysical properties depend on many parameters such as the glass composition, the temperature, the dissolved gas partial pressure, and the composition and pressure of the atmosphere [10]. According to Kawachi and Kawase [5] reliable data and measurement methods are not yet available for some of the thermophysical properties needed. The purpose of this work is neither to develop and extensive database nor to provide new experimental results or measurements methods. Instead, its specific aim is to collect and assess the available data for soda-lime silicate glass. Particular attention was paid to the properties of the most common composition ($74SiO_2$–$16Na_2O$–10CaO (mol%)) of soda-lime silicate glass or similar compositions over the temperature range of 1000–2000 K. The thermophysical properties of the molten glass have been previously reported [11] and need not be reproduced. Discussion of the gas physicochemical properties used as input parameters to the numerical simulations is included in the next subsection and is limited to oxygen and carbon dioxide gases. Additional data for nitrogen, water vapor, and sulfur dioxide are given in Ref. [12].

2.1. Surface tension

The surface tension depends on the temperature, the bulk glass composition, the atmosphere composition, and the ions dissolved in the melt such as the sulfate [13]. The effect of all those parameters are discussed in detail

by Schulze [10]. In brief, surface tension decreases with increasing temperature and the fraction of CaO and Na_2O. The surface tension of the system $74SiO_2$–$16Na_2O$–10CaO (mol%) soda-lime silicate glass/air is given by [10,14],

$$\sigma(T) = 321.7 - 0.04 \times (T - 1173.15) \quad \text{in mN/m}. \tag{1}$$

The above expression is assumed to be independent of the gas, i.e., Eq. (1) is used for both carbon dioxide/ and oxygen/soda-lime silicate glass systems. However, it has been observed experimentally that the surface tension of soda-lime silicate glass was reduced by the presence of gases having a non-zero dipole moment in the atmosphere [15]. Water vapor has been identified as having the most significant effect on the surface tension. At temperatures larger than 600 °C, however, the effect of water vapor has been considered to be negligible [10,13]. The effect of the atmosphere on the surface tension is of great importance in the formation of glass foam [13,16], and even a small surface tension depression can have a significant effect on the foam thickness as shown experimentally by Ghag et al. [17] for water + 78% glycerin solution. Unfortunately, no data are reported in the literature for the change of surface tension with water vapor pressure at high temperatures; therefore, this effect will not be considered further.

2.2. Gas diffusion coefficient in the glassmelt

The most extensive diffusion measurements have been made for fused silica, since this glass is one of the most permeable to gases. Unfortunately, for other types of glass, a few measurements concerning gases other than helium and hydrogen are available [18]. The variation of the diffusion coefficient of the gas species 'i' in a glassmelt as a function of temperature is known to follow an Arrhenius type of law [19]:

$$D_i = D_{0,i} \exp(-\Delta H_{D,i}/RT), \tag{2}$$

where $D_{0,i}$ and $\Delta H_{D,i}$ are empirically determined constants.

Diffusion coefficient of oxygen in the molten glass varies significantly from one type of glass to another as shown by Doremus [20]. Very often the soda-lime silicate glass composition was not available even though it is well known that the gas diffusion coefficients and solubilities can depend significantly on the glass composition. A fit of the experimental data presented by Terai and Oishi [21] gives the following expression for the diffusion coefficient of oxygen in $71.7SiO_2$–$15.5Na_2O$–12.8CaO (mol%) soda-lime silicate glass:

$$D_{O_2} = 3.2 \times 10^{-6} \exp(-21\,076/T). \tag{3}$$

A fit of data reported by Doremus [20] for a commercial soda-lime silicate glass leads to the following expression:

$$D_{O_2} = 1.14 \times 10^{-3} \exp(-24\,946/T). \tag{4}$$

Unfortunately, the composition of the glass studied by Doremus [20] is unknown and it is believed to contain other elements such as MgO and Al_2O_3 [19]. The discrepancies among experimental data are assumed to be due the differences in the glass compositions. It was decided to use the data reported by Terai and Oishi [21] since they cover a wider range of temperatures, and the glass studied has a very similar composition to that of interest in the present study, i.e., $74SiO_2$–$16Na_2O$–10CaO (mol%).

The only additional information available in the literature concerning the diffusion coefficient of carbon dioxide in soda-lime silicate glass is the following expression proposed by Nemec and Muhlbauer [22],

$$D_{CO_2} = 7.95 \times 10^{-9} \exp[-11\,332/(T - 473.4)]. \tag{5}$$

2.3. Gas solubility in the glassmelt

Gases can dissolve in the glassmelt by physical and/or chemical dissolution. Physical dissolution consists of occupying free spaces in the network of the molten glass. Physical solubility is higher for small gas molecules and increases slightly with temperature [10]. Gases can also dissolve chemically, i.e., they react chemically and create bonds with the glass structure.

Solubility is the amount of dissolved gas per unit mass of melt per unit of applied pressure and is expressed in many different units. The common unit is the volume of gas at standard temperature and pressure (STP, 0 °C and 1 atm) per unit volume of material exposed at one atmosphere of gas (m^3 (STP)/m^3 atm). It can also be expressed in kg/m^3 Pa. Doremus [18] pointed out that these definitions contain implicitly a temperature dependence since the applied pressure follows the ideal gas law, $P = nRT/V$. Instead, Doremus [18] suggested the use of 'Ostwald solubility' defined as the ratio of the concentration of the gas in the material C_i and the concentration of the gas in the surrounding atmosphere C_g,

$$S_{i,Os} = \frac{C_i}{C_g}. \tag{6}$$

In the present work, however, solubility will be expressed in moles of gas per unit volume of liquid phase per unit external partial pressure of the gas (mol/m^3 Pa) as used in the most common form of the Henry's law. The relationships between the different units for solubility are

$$1\ [\text{mol/m}^3\,\text{Pa}] = \frac{1}{RT_{STP}} \quad [\text{m}^3\,(\text{STP})/\text{m}^3\,\text{atm}] = \frac{1}{RT} S_{i,Os}, \tag{7}$$

where R is the universal gas constant ($= 8.314$ J/mol K), T is the temperature, and T_{STP} is the temperature at the

standard atmosphere (= 273.15 K). In the following sections the solubility is expressed in mol/m^3 Pa and is assumed to follows an Arrhenius type of law:

$$S_i = S_{0,i} \exp(\Delta H_{S,i}/RT), \tag{8}$$

where $S_{0,i}$ and $\Delta H_{S,i}$ are constants determined experimentally.

The solubility of oxygen depends strongly on the glass composition [23]. The presence of suitable elements of variable valence such as antimony oxide or arsenic can increase the solubility [23]. The only collected data concerning the solubility of oxygen in soda-lime silicate is [23]

$$S_{O_2} = 2.2 \times 10^{-4} \quad \text{in mol/m}^3\,\text{Pa}. \tag{9}$$

An expression of solubility of carbon dioxide is available in the literature and compares well with reported experimental data [22]:

$$S_{CO_2} = 3.45 \times 10^{-6} \exp(3840/T) \quad \text{in mol/m}^3\,\text{Pa}. \tag{10}$$

2.4. Refining reactions

The present study is concerned with antimony pentaoxide used as the refining agent and decomposing according to the reaction $Sb_2O_5 \rightleftharpoons Sb_2O_3 + O_2\uparrow$. Kawachi and co-workers [4,5,24] showed that the rate of the backward reaction can be neglected in the production of TV-panel glass. Therefore, the refining reaction can be considered as irreversible with only the decomposition of Sb_2O_5 taking place. Reaction rate constants and order of the refining reaction involving antimony oxide in TV-panel glass can be found in the literature [24]. The same refining reaction characteristics were assumed to hold also for soda-lime silicate glasses. Antimony oxide is considered for the following reasons: the refining reaction produces only oxygen whose concentration in the glassmelt has to be computed, and the reaction is complete and irreversible so that refining agent concentration can be computed independently from the dissolved gas concentrations $C_{\infty,i}$ and the bubble density function f_1. Treatment of equilibrium refining reactions, such as these involving sodium sulfate Na_2SO_4, would consists of including the computation of the refining agent concentration into the iterative scheme for the dissolved gas concentrations and the bubble density function to account for their interdependence. In addition, when sodium sulfate is used as a refining agent both oxygen and sulfur dioxide SO_2 are generated during the refining process. Then, they dissolve in the glassmelt and can diffuse in and out of the bubbles [13,25]. Therefore, concentrations of both oxygen and sulfur oxide dissolved in the molten glass and their molar fractions in the bubbles should be computed along with those of carbon dioxide. The bubbles are then characterized by six independent variables (e.g., x, y, z, r, γ_{CO_2}, γ_{O_2}) making the numerical scheme quite involved. Such a situation falls beyond the scope of the present study whose main objective is to demonstrate the feasibility of the calculations.

Finally, it has not been possible to find the diffusion coefficient of the refining agent in soda-lime silicate glass.

3. Results and discussion

3.1. Model glass tank and parameters

The same glass melting tank as that used for three-dimensional flow and thermal structures of molten glass was considered [11,26]. It is a rectangular bath 15.85 m long, 7.315 m wide, and 1.03 m deep (see Fig. 1). The molten glass exits the tank through a throat having a cross-sectional area of 0.386×0.802 m^2 which is located at the bottom and in the middle of the front wall. The raw batch material leading to a glassmelt of composition of $74SiO_2$–$16Na_2O$–$10CaO$ (mol%) is introduced into the tank at a rate $\dot{m}_b$ of 356 tons/day (or 4.12 kg/s) in the form of a loose blanket covering the entire width of the tank. Since about 200 kg of gases are produced per ton of batch introduced [27], the corresponding glass production rate (pull rate) $\dot{m}_{pull}$ is 297 tons/day (or 3.347 kg/s) of molten glass.

The simulations consider an oxy-fuel furnace burning methane and oxygen at stoichiometric conditions at atmospheric pressure according to reaction $CH_4 + 2O_2 \rightarrow 2H_2O + CO_2$. Thus, the partial pressures of oxygen and carbon dioxide at the glassmelt/combustion space interface are taken as 0.0 and $p_0/3$, respectively.

The energy ΔH_{melt} required to bring the batch from room temperature (320 K) to clear molten glass and the melting temperature T_{melt} were taken equal to 2200 kJ/kg and 1450 K, respectively [28]. A linear decrease of the glassmelt velocity at the batch/glassmelt interface from 0.2 cm/s where the batch enters the furnace to zero at the tip of the batch blanket was chosen to simulate the fact that the batch blanket becomes thinner and less compact from the loading end to the tip. The maximum batch

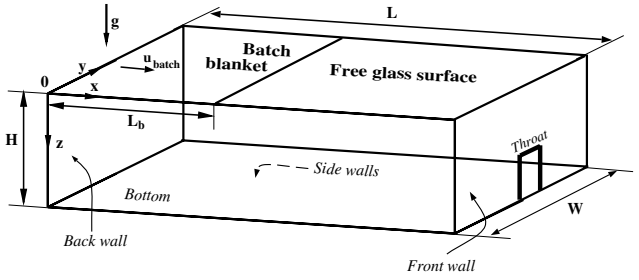

Fig. 1. Schematic of the modeled glass melting tank and the associated systems of coordinates.

velocity of 0.2 cm/s was computed based on the pull rate of 4.12 kg/s for a batch blanket covering the entire width and having a density of 1400 kg/m^3 and a thickness of 20 cm. Moreover, from previous work [26] based on the momentum equation for a batch blanket at rest projected onto the vertical axis, a depth of 10.4 cm of the batch blanket was assumed to be submerged under the free glass surface.

The heat losses between the glassmelt and the ambient surroundings through the walls were computed assuming 1-D heat conduction through the refractories and cooling of the walls by natural convection using an ambient temperature of 320 K. The construction of the sidewall refractories were considered to be the same, with an overall heat transfer coefficient of 3.86 W/m^2 K. At the bottom of the tank the overall heat transfer coefficient equals 3.89 W/m^2 K and that at the back and front wall is equal to 5.57 W/m^2 K.

The net heat flux incident from the combustion space and reaching the surface of the batch and of the molten glass is assumed to have the longitudinal profile shown in Fig. 2, where the parameters $q''_{\max}$ and q''_0 are the maximum heat flux and the heat flux at the back wall ($x = 0$ m), respectively. The distance from the back wall to the location of the maximum heat flux is $L_{\max}$ and the distance where the heat flux vanishes is L_0. They were assumed to be equal to 7.5 and 13.84 m, respectively. Such a heat flux profile was chosen based on industrial practices [11]. The three-dimensional flow and thermal structures of the molten glass for the above conditions have been presented and discussed in details in Refs. [11,26] and need not be repeated here. Only the temperature, velocity, and streamlines at midplane in the longitudinal direction are reproduced in Fig. 3. One can see that a part of the pull current flows directly from under the batch along the bottom of the tank to the throat as experimentally observed by Zhiqiang and Zhihao [29]. Thus the product quality is expected to be degraded due to the shorter residence time of the glassmelt in the tank.

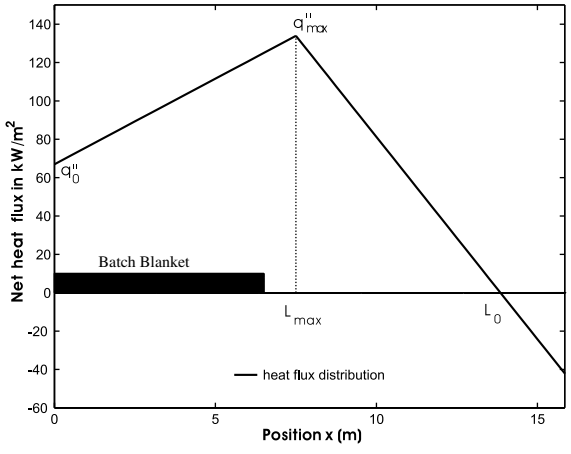

Fig. 2. Heat flux distribution used as the boundary condition at the glassmelt/combustion space interface.

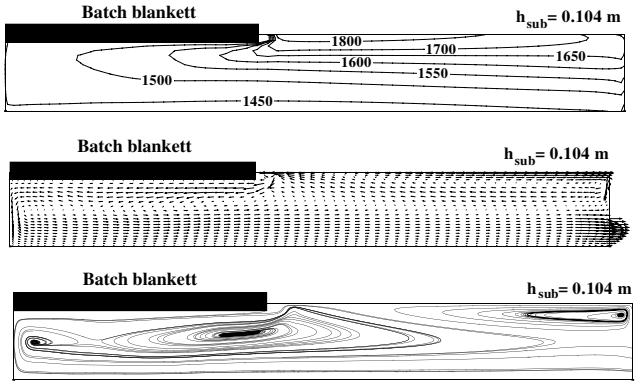

Fig. 3. Flow field used as input parameter with from top to bottom (top) velocity field, (center) temperature field, and (bottom) streamtraces at the tank midplane.

3.2. Analysis of the results

The calculations yield the value of the bubble density function f_1, the bubble radius r, and the molar fraction of each gas contained in the bubbles γ_i at each scalar nodes as well as the concentration(s) of gas(es) dissolved in the melt. The amount of information obtained from the computer program is very large and not easily interpretable unless it is reduced to physical quantities. Therefore, for a better interpretation of the computational results the bubble density function f_1 and the bubble radius r were converted into more physical and understandable local variables such as the total number of bubbles N, the interfacial area concentration A_i, the volume fraction of the gas phase f_v, the average bubble radius $\bar{r}$ and the average carbon dioxide molar fraction $\bar{\gamma}_{CO_2}$ at each scalar grid point (x_I, y_J, z_K). For bubbles containing a single gas or a diffusing and a non-diffusing gas, only one independent internal variable (r) is considered and N, A_i, f_v, $\bar{r}$, and $\bar{\gamma}_{CO_2}$ are defined, respectively, as

$$\text{0th moment} \quad N(x,y,z) = \int_0^\infty f_1(x,y,z,r)\,\mathrm{d}r, \tag{11}$$

$$\text{1st moment} \quad \bar{r}(x,y,z) = \left[\int_0^\infty r f_1(x,y,z,r)\,\mathrm{d}r\right] \Big/ N(x,y,z), \tag{12}$$

$$\text{1st moment} \quad \bar{\gamma}_{CO_2}(x,y,z) = \left[\int_0^\infty \gamma_{CO_2} f_1(x,y,z,r)\,\mathrm{d}r\right] \Big/ N(x,y,z), \tag{13}$$

$$\text{2nd moment} \quad A_i(x,y,z) = \int_0^\infty 4\pi r^2 f_1(x,y,z,r)\,\mathrm{d}r, \tag{14}$$

$$\text{3rd moment} \quad f_v(x,y,z) = \int_0^\infty \frac{4\pi r^3}{3} f_1(x,y,z,r)\,\mathrm{d}r. \tag{15}$$

In the case of single component gas bubbles $\bar{\gamma}_{CO_2}(x,y,z,r) = 1$. If several diffusing gases are treated, additional internal variables have to be considered and the above integrals become multiple integrals with respect not only to variable r but also to other internal variables γ_i. Note also that, unlike discretized formulations previously suggested [3], which divide the bubble size distribution in groups and solve the population balance equation for the number of bubbles in each group, the present formulation and the associated method of solution compute directly the bubble density function f_1 enabling accurate predictions of any moments of the density function and in particular the zero (N), first ($\bar{r}$ and $\bar{\gamma}_{CO_2}$), second (A_i), and third (f_v) order moments. The above single integrals are computed numerically using the Simpson's rule of integration for unequally spaced data [30].

3.3. Numerical method

In order to validate the numerical implementation of the backward method of characteristics, computations of the bubble radius and density function for simple physical situations having closed-form analytical solutions have been performed [31]. Very good agreement between numerical predictions and analytical solutions for r, and f_1 have been reported for one and two dimensional flows and both transient and steady-state situations [31].

Numerical difficulties arise due to the fact that many key variables (e.g., the pressure inside the bubbles p_b) are functions of $1/r$ which tend to infinity as the bubble radius decreases. However, extremely small bubbles cannot be physically treated in the same manner as macroscale bubbles due, for example, to gas rarefaction effects, and the limits of the concept of surface tension at very small scale. To avoid numerical problems and account for physical limitations of the model, bubbles are considered to disappear when their radius becomes less than 1.0 μm as suggested by Kawachi and Kawase [5]. Then, the bubble radius r and the bubble density function f_1 are arbitrarily set to 1.0 μm and zero, respectively, corresponding effectively to a sink term in the bubble population balance equation.

The grid sensitivity study for the spatial discretization has been previously performed for the velocity and temperature fields [11]. The entire glass bath was discretized using the $66\times39\times25$ staggered grid used for computing the glassmelt flow and thermal structures [11,26]. The same grid was used for the refining agent concentration and the concentrations of gases dissolved in the molten glass. The steady state was estimated to be reached when the residual for these variables fell below an arbitrarily small constant ϵ_1. The steady-state for the bubble density function f_1, the bubble radius r, and the gas molar fraction γ_{CO_2} is assumed to be reached when the maximum relative variation of the predicted variables between two consecutive iterations over the computational domain fall under an arbitrarily small constant ϵ_2, i.e.,

$$\max\left[\frac{|X_{I,J,K}^{(n-1)} - X_{I,J,K}^{(n)}|}{|X_{I,J,K}^{(n-1)}|}\right] \leqslant \epsilon_2 \quad \text{for } 1\leqslant I\leqslant 66, 1\leqslant J\leqslant 39, \text{ and } 1\leqslant K\leqslant 25, \tag{16}$$

where n denotes the iteration number, X is the general symbol for r, f_1, and γ_{CO_2}, while I, J, K are the indices for the scalar nodes of the staggered grid in the x-, y-, and z-directions, respectively. Numerical results for $C_{\infty,i}$, r, f_1, and γ_{CO_2} at steady state were found to be independent of ϵ_1 and ϵ_2 provided that $\epsilon_1 \leqslant 10^{-5}$ and $\epsilon_2 \leqslant 4\times10^{-3}$.

Moreover, in order to reduce computational time and still provide adequately accurate results, grid sensitivity studies have been conducted to choose the suitable number of points taken on the initial bubble density function that gives grid-independent numerical results for N, A_i, $\bar{r}$, $\bar{\gamma}_{CO_2}$, f_v, and C_{∞,CO_2}. Numerical sensitivity tests have been made with 6, 11, and 22 points on the initial bubble density function as represented in Fig. 4. For all simulations, the results N, A_i, $\bar{r}$, and f_v, for the same simulated time differed by less than 1.5% between 11 and 22 points. Therefore, 11 points on the initial distribution are sufficient to obtain a solution independent of the number of points considered on the initial distribution. The time step was proven to have no influence on the final results as long as at least two consecutive points on the pathlines are contained in any elementary computational volume of the $66\times39\times25$ staggered grid [31].

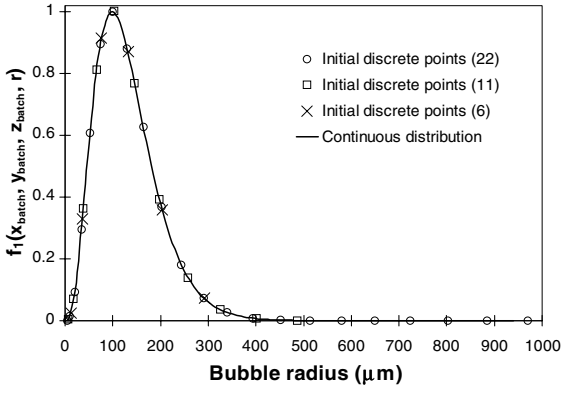

Fig. 4. Initial bubble density function under the batch and arbitrary discrete set of points chosen for the simulations (Eq. (17)).

Unfortunately, no experimental data for full scale industrial glass melters are available to quantitatively validate the numerical results. Comparison with numerical results reported in the literature [3,5,6] were made when available. Such comparison with results for the local number of bubbles obtained by Balkanli and Ungan [3] may be misleading since, as pointed out in the first part of the study [1], the boundary conditions used, the expression for the time rate of change of bubble radius, the decoupling of the gas concentration and the bubble population balance equations are questionable. Moreover, the method of solution based on the discretized formulation cannot predict accurately the other moments of the bubble density function such as $\bar{r}$, $\bar{\gamma}_{CO_2}$, A_i, and f_v [32,33]. The next two sections present results of sample calculations for the physical situations when bubbles contain only CO_2 and when bubbles contain both CO_2 as a non-diffusing gas and O_2 as a diffusing gas, respectively.

3.4. Bubbles containing a single gas

Previous studies solving the bubble population balance equation have been concerned only with carbon dioxide bubbles and have neglected the coupling between the concentration of gas dissolved in the molten glass and the bubble population balance equation [3]. This assumption has been made for the sake of simplicity but has not been justified on physically or numerically sound arguments. However, the gas contained in single component gas bubbles can only diffuse out of the bubbles since the gas concentration at the bubble/glassmelt interface at equilibrium $C_{e,i}$ given by the Henry's law is always larger than the gas solubility in the glassmelt (Ref. [1], Eq. (25)). Bubbles shrink due to gas diffusion while they can grow or shrink due to pressure changes; therefore, the presence of bubbles may be a significant source for the gas dissolved in the molten glass and decoupling the gas concentration and the bubble density function may not be appropriate. This section presents and discusses the results when carbon dioxide is the only diffusing gas considered. It represents a limiting case of practical applications since even when no refining agent is added to the batch, water vapor generated in the combustion space, which has a large diffusion coefficient and solubility in the glassmelt [19], dissolves in the melt and diffuses in the bubbles. The situation considered is highly idealized in order to (1) show the feasibility of the calculations, (2) compare with similar simulations previously reported in the literature [2,3,7], and (3) assess the effect of bubbles on the concentration of gases dissolved in the molten glass that was neglected in previous studies [2,4–6].

The size distribution of bubbles generated by fusion/melting of the raw materials and used as a boundary condition is assumed to follow a gamma distribution defined as

$$f_1(\vec{x}_{batch}, r, t) = Ar^{\eta} \exp(-Br); \tag{17}$$

the three constants A, B, and η are positive and real numbers determined from experimentally measured quantities such as the radius r_{max} at which the density function reaches a maximum, the total number of bubbles per unit volume of liquid N, and the volumetric void fraction f_v. These quantities can be related to the constants A, B, and η by

$$r_{max} = \left(\frac{\eta}{B}\right), \quad N = \frac{A\Gamma(\eta+1)}{B^{(\eta+1)}}, \quad \text{and}$$
$$f_v = \frac{4\pi A\Gamma(\eta+4)}{3B^{(\eta+4)}}, \tag{18}$$

where $\Gamma(z)$ is the gamma function ($\Gamma(z) = \int_0^\infty e^{-t}t^{z-1}\,dt$) which has been tabulated by Abramowitz and Stegun [34]. Based on experimental results reported in the literature [5,35,36], r_{max}, N, and f_v under the batch were taken to be 98 μm, 2240 bubbles per cubic centimeter of glass, and 4%, respectively, leading to constants $A = 3.23 \times 10^{26}$ m^{-7}, $B = 3.05 \times 10^4$ m^{-1}, and $\eta = 3$. The corresponding average bubble radius and interfacial area concentration are 112 μm and 609 m^2/m^3 of glass, respectively. Note that the problem of conservation of the total number of bubbles raised in the first part of the study is not of concern here since the bubble growth/shrinkage rate is very small, owing to the small diffusion coefficient and solubility of carbon dioxide in the glassmelt and due to the small temperature and viscosity gradients, i.e., $\partial w_r/\partial r \approx 0.0$ (see Eq. (52) in Ref. [1]), as checked and confirmed numerically.

First, numerical simulation for the CO_2 concentration in the glassmelt neglecting the presence of bubbles has been performed. Fig. 5(a) shows the concentration of carbon dioxide dissolved in the glass bath obtained at the midplane. The figure reveals a fairly uniform carbon dioxide concentration along the glass bath with a sharp concentration gradient close the glass free surface. The relatively uniform carbon dioxide concentration can be explained by the good mixing caused by advective currents and indicates that advection dominates over diffusion [7]. The dominance of advection over diffusion explains also the sharp concentration gradient under the glassmelt surface since in this region the molten glass flows parallel the free surface and transport of carbon dioxide in the normal direction (z-direction) takes place only by diffusion. The lower concentration at the surface of the glass bath is due to the fact that solubility decrease exponentially with temperature (see Eq. (10)). The temperatures at the glass free surface are larger than those under the batch by about 250 K [26]. Thus, the CO_2 concentration imposed at the glassmelt/combustion space interface is much smaller than that imposed at the glassmelt/batch interface. Overall, numerical predictions of the CO_2 concentration agree well with those reported by Balkanli and Ungan [7]. However, these authors

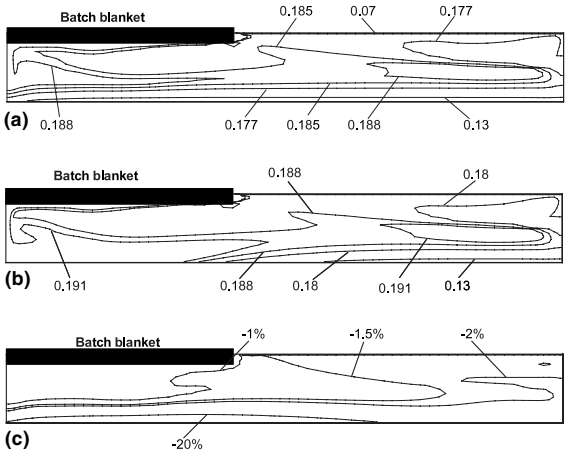

Fig. 5. Dissolved CO_2 gas iso-concentration lines at midplane in kg/m^3 (a) without accounting for the presence of bubbles and (b) with accounting for the source term due to gas diffusion in and out of bubbles, and (c) relative difference (in %) between the local CO_2 concentrations in (a) and (b).

while using the same boundary conditions and the same expression for the carbon dioxide solubility as those of the present study did not mention the partial pressure of carbon dioxide at the glassmelt/combustion space interface used in their numerical simulations. The value of 0.001 kg/m^3 they reported at the glass surface tends to indicate that they imposed a very small partial pressure of CO_2 at the glassmelt/combustion space interface, whereas it should be fairly large since CO_2 and water vapor are the main products of the combustion.

Second, the CO_2 concentration is computed by accounting for the source term owing to CO_2 diffusion out of the bubbles. A converged solution was obtained after two full successive calculations for the CO_2 concentration C_{∞,CO_2} in the glassmelt and the bubble radius r and density function f_1. Fig. 5(b) shows the concentration of carbon dioxide dissolved in the glass bath at the midplane, while Fig. 5(c) shows the relative difference in the CO_2 concentration between Fig. 5(a) and (b). It indicates that accounting for gas diffusion out of the bubbles as a source term for carbon dioxide dissolved in the glassmelt does not significantly change the numerical results and the CO_2 concentration increases by less than 2% in most of the glass bath when diffusion out of the bubble is accounted for. Similar spatial distribution of iso-concentration lines can be obtained by shifting the concentration by +0.003 kg/m^3. For example, the 0.185 kg/m^3 iso-concentration line when the presence of bubbles is neglected has a profile similar to the 0.188 kg/m^3 concentration line when the presence of bubbles is accounted for.

Finally, note that supersaturation (up to 50%) of the glassmelt with CO_2 occurs under the batch and at the bottom of the tank (see Fig. 6). This could lead to heterogeneous bubble nucleation if a large enough amount

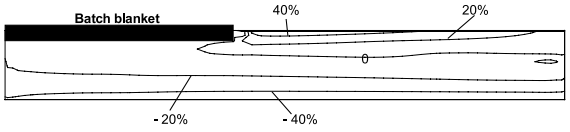

Fig. 6. Relative difference between the local CO_2 saturation and CO_2 concentration (in %) at midplane accounting for the source term due to gas diffusion in and out of bubbles (negative values correspond to supersaturation).

of undissolved sand grains is present in this region. Bubble nucleation could then result in secondary foam formation in the region beyond the batch tip as commonly observed in industrial glass melting furnaces [13]. Then, secondary foam would be generated not only by bubbles rising from the glassmelt but also from bubbles generated due to oversaturation of the glassmelt and nucleation at the unmelted sand grain surface. However, it is beyond the scope of the present study to investigate such a complex phenomena.

The hypothetical situation in which bubbles would be injected at the batch/glassmelt interface at time $t = 0$ s and would grow or shrink and be transported in the glassmelt by advection currents has been simulated. Fig. 7 shows a series of iso-concentration lines for the total number of bubbles per unit volume of glass N at midplane for 1, 2, 3, and 4 h after the beginning of injection. The iso-concentration lines propagates with the glass flow from under the batch to the front wall and then move up toward the free surface before sinking again under the batch. It clearly shows the transport of

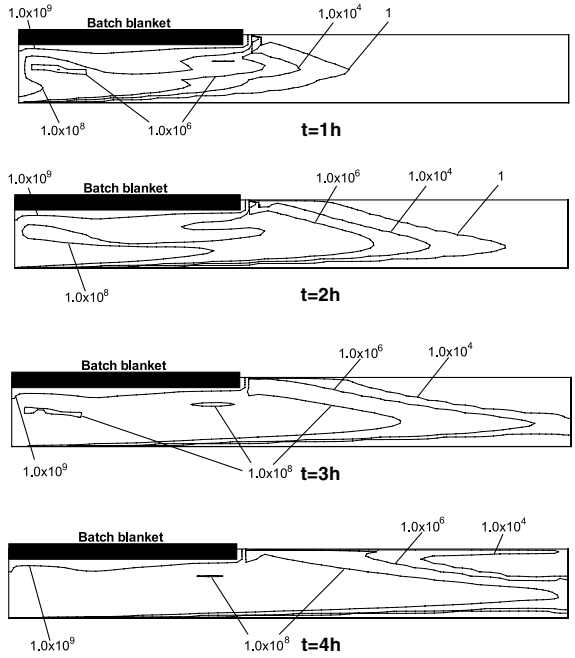

Fig. 7. Evolution of iso-concentration lines with time for the total number of bubbles N (in #/m^3) at midplane.

bubbles by convective currents from under the batch to the refining section and the throat. It also demonstrates the capability of the computer program based on the backward method of characteristics to simulate transient problems. Convergence to steady state is very slow owing to the complexity of the flow field, the small velocities of the glassmelt, and the slow transport phenomena taking place in the glassmelt. In industrial glass melting furnaces, it is estimated that it can take up to two days for a glassmelt fluid particle to flow from under the batch to throat corresponding to 320 000 time steps to be computed for each points taken on the initial bubble size distribution (see Fig. 4).

Numerical results for the total number of bubbles at steady-state at different cross-sections in the longitudinal direction are shown in Fig. 8. One can observe the predominance of the bubble transport in the longitudinal direction and no significant changes in the profile of the total number of bubbles from the midplane ($y/W = 0.5$) to the side wall ($y = W = 0.01$) are evident. Moreover, the total number of bubbles entrapped in the glassmelt is large and relatively uniform due to the small diffusion coefficient of CO_2 in the glassmelt and the good mixing provided by convection currents.

The steady-state numerical results for the total number of bubbles N, the average bubble radius $\bar{r}$, the interfacial area concentration A_i, and the void fraction f_v, respectively at the midplane ($z/W = 0.5$) are presented in Fig. 9(a)–(d) and correspond to a simulated time of 48 h. As one can see,

- A large number of bubbles remain in the glassmelt including near the glassmelt free surface.
- The average bubble radius decreases slightly as the bubbles are transported by the convection currents from under the batch to the refining section owing to the small diffusion coefficient of CO_2 in the glassmelt.
- A large bubble concentration gradient exist near the free surface since only large bubbles escape to the free glassmelt surface. Indeed, the glassmelt flowing near the free surface from the hot spot toward the batch prevents the smallest bubbles from reaching the surface. These bubbles are too small for the buoyancy force to overcome the strong convection currents in the horizontal plane near the surface of the molten glass. Thus, small bubbles get trapped in the first recirculation loop located in the first half of the tank and significantly fewer bubbles are trapped in the second recirculation loop located closed to the front wall.
- Finally, Fig. 9(a) and (b) indicate that a large number of bubbles with an average diameter between 70 and 100 μm are transported from the batch through the submerged throat as they are carried by advection when the glassmelt is being pulled. Note also that the average bubble diameter increases near the throat. This is attributed to gas expansion due to the increase of the bubble temperature as they rise back to the glassmelt surface after being carried along the bottom of the tank. This results in a poor glass quality and productivity but was expected given the glassmelt flow pattern discussed earlier. It is, therefore, interesting to investigate the impact of the refining agent on the bubble behavior since refining gases diffuse in the bubbles to enable the bubbles to rise to the glassmelt surface by buoyancy before reaching the throat.

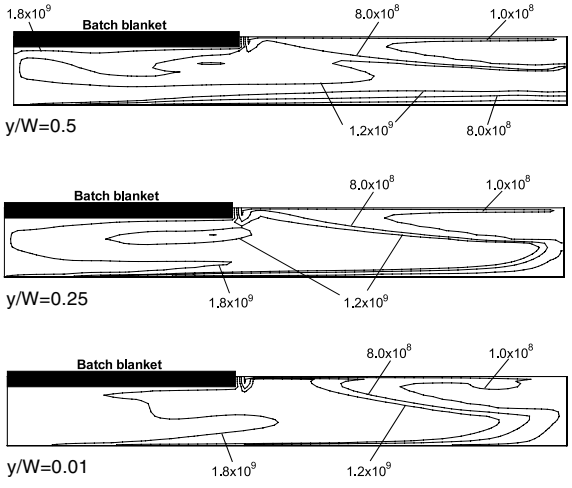

Fig. 8. Steady-state iso-concentration lines for the total number of bubbles N (in #/m^3) at midplane $y/W = 0.5$ (top), at $y/W = 0.25$ (center), and $y/W = 0.01$ (bottom).

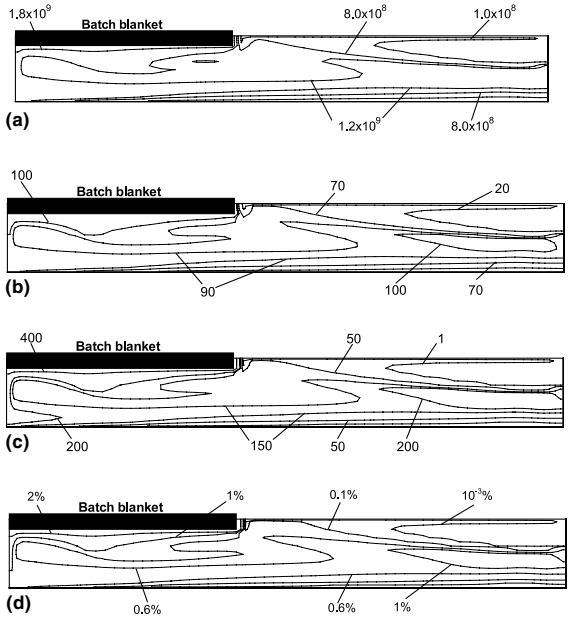

Fig. 9. Iso-concentration lines at midplane for (a) N (in #/m^3), (b) $\bar{r}$ (in μm), (c) A_i (in m^2 of interface/m^3 of glassmelt), (d) f_v (in m^3 of gas in bubbles/m^3 of glassmelt) at midplane.

3.5. Bubbles containing two different gases

Bubble growth in the glassmelt can only be due to the diffusion of gases such as oxygen, water vapor, and sulfur oxide that have a large diffusion coefficient and a large enough solubility [37]. Bubble growth is obtained by adding refining agents to the batch that produce such gases. The present example is limited to the important practical situations when antimony pentoxide Sb_2O_5 is added to the raw batch materials as a refining agent. The refining agent concentration is needed to compute the oxygen concentration dissolved in the glassmelt and diffusing in and out of the bubbles. It can be computed independently from the other variables since refining reactions are assumed to be irreversible and complete. However, since the diffusion coefficient of the refining agent and the reaction rate constants of the refining reaction involving antimony oxide in soda-lime silicate glass could not be obtained from the literature, the refining agent concentration has not been computed. Instead, the oxygen concentration dissolved in the glassmelt was assumed to be equal to saturation at the local temperature and pressure everywhere in the glass bath. This can be justified by the fact that oxygen is supplied in great amount during the melting of batch. Thus, its concentration in the glassmelt under the batch should be uniform as shown for CO_2. Furthermore, unlike CO_2, oxygen is also generated by refining reactions in the refining section of the tank where the temperatures are large allowing refining reactions to occur. Finally, convection currents produce good mixing that leads to uniform oxygen concentration in the glassmelt similar to that observed for carbon dioxide. The same sharp concentration gradient at the glassmelt/combustion space interface observed for CO_2 is expected for O_2 since the boundary condition for the oxygen concentration is $C_{\infty,O_2} = 0.0$ at the glassmelt/combustion space interface. This concentration gradient is neglected since it is very sharp and highly localized to a small depth in the glassmelt.

In the case under consideration, both carbon dioxide and oxygen dissolved in the glassmelt or contained in the bubbles have to be considered. Carbon dioxide is generated during the melting of calcium carbonate while oxygen is released by the decomposition of nitrates such as $NaNO_3$ and of the refining agent [25]. For a typical soda-lime silicate glass batch without refining agent, experimental analysis of gases released during batch melting and fusion [38,39] indicate that significantly more (at least 15 times) CO_2 is generated than other gases. But, oxygen is generated by refining reactions. Therefore, as a first order approximation, bubbles located under the batch are assumed to contain both CO_2 and O_2 at equal molar fraction, i.e., $\gamma_{CO_2} = \gamma_{O_2} = 0.5$, at the batch/glassmelt interface. Since the diffusion coefficient and solubility of carbon dioxide are at least one order of magnitude smaller than those of oxygen [37,40,41] over the temperature range 1000–2000 K, carbon dioxide is treated as a non-diffusing gas and only oxygen is assumed to diffuse in and out of the bubbles. This assumption has the advantage of simplifying the numerical algorithm by avoiding two-dimensional numerical integration from scattered data points for the amount of gas diffusing from the glassmelt to the bubbles $\dot{m}_{diff}$ (see part I [1], Eq. (15)). Such integration would require bivariate interpolation and smooth surface fitting onto an equally space fixed grid for initial values given at irregularly distributed points [42,43], before performing the double integration by repeated one-dimensional numerical integration using Simpson's rule [30].

Moreover, the number of moles of carbon dioxide contained in the bubbles remains constant while the CO_2 molar fraction changes due to oxygen diffusion. The CO_2 molar fraction in the bubbles at location z having radius r and temperature T is expressed as

$$\gamma_{CO_2} = 1 - \gamma_{O_2} = \frac{T(p_0 + 2\sigma/r_0)}{T_{melt}(p_0 + \rho_\infty g z + 2\sigma/r)} \left(\frac{r_0}{r}\right)^3 \gamma^0_{CO_2}. \tag{19}$$

The initial bubble radius of a point of the initial bubble density function under the batch is denoted r_0. The initial bubble temperature equals the batch melting temperature T_{melt} taken as 1450 K. Finally, the initial molar fraction of CO_2 in the bubbles is given by $\gamma^0_{CO_2}$ while the bubbles are assumed to be initially located in the plane $z = 0$ m. Since CO_2 is assumed not to diffuse in or out of the bubbles, the bubbles can shrink until the molar fraction of CO_2 becomes unity and the bubble radius reaches its minimum r_{min}, which can be determined by solving the following equation:

$$(p_0 + \rho_\infty g z) r^3_{min} + 2\sigma r^2_{min} - (p_0 r_0^3 + 2\sigma r_0^2) \frac{T}{T_{melt}} \gamma^0_{CO_2} = 0. \tag{20}$$

Fig. 10(a)–(d) show the numerical results for the total number of bubbles per unit volume of glass N, the average bubble radius $\bar{r}$, the average molar fraction of CO_2, the interfacial area concentration A_i, and the volumetric gas fraction f_v. As one can see, most of the bubbles are located under the batch where the interfacial area concentration and the void fraction are the largest. Compared with the case when only CO_2 is considered one can conclude that (1) less and smaller bubbles are present in the glassmelt and particularly near the glassmelt surface and at the throat, (2) bubbles are more located around the batch blanket and do not cover the entire glassmelt surface, (3) the average diameter of bubbles leaving the tank at the throat is between 10 and 60 μm compared with 70–100 μm when only CO_2 is considered, (4) the average CO_2 molar fraction (not

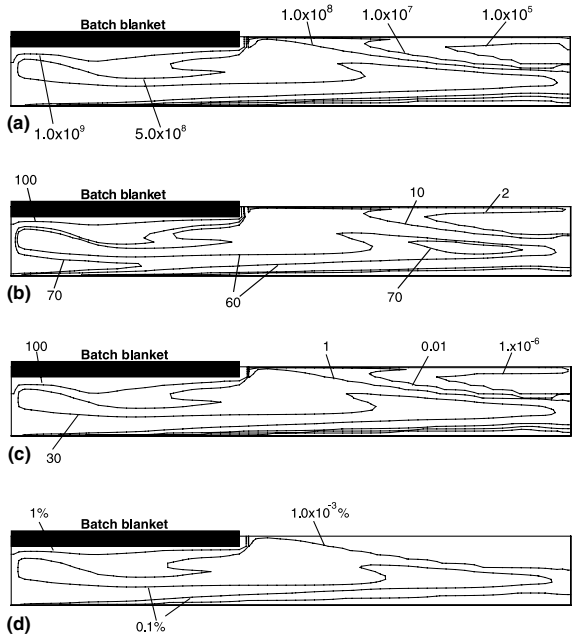

Fig. 10. Iso-concentration lines at midplane for (a) N (in #/m^3), (b) $\bar{r}$ (in μm), (c) A_i (in m^2 of interface/m^3 of glassmelt), (d) f_v (in m^3 of gas in bubbles/m^3 of glassmelt).

plotted here) increases relatively quickly as bubbles move away from the batch blanket and is almost uniform across the glass bath. This can be explained by the fact that oxygen diffuses out of the bubbles much faster than carbon dioxide ($D_{O_2} > D_{CO_2}$). Therefore, the main mechanism of refining is bubble dissolution or absorption. Similar results have been also obtained numerically by Kawachi and Iwatsubo [6] for similar simulated conditions when the hot spot was located at about 2/3 of the total furnace length and the concentration of oxygen dissolved in the glassmelt was large and almost uniform.

4. Conclusions

This paper presents numerical results for sample calculations of bubble transport, growth or shrinkage in three-dimensional laminar gravity driven flow based on the model presented in details in the first part with applications to glass melting furnaces. The following conclusions can be drawn:

- The present study demonstrates the feasibility of solving the bubble population balance equation in three-dimensional laminar gravity driven flow for both transient and steady-state situations using the backward method of characteristics.
- Detail calculations of the bubble density function enables one to compute any mth order moments of the density function and in particular, the total number of bubbles, the average bubble radius, the average gas molar fraction, the interfacial area concentration and the void fraction.
- Due to the small liquid velocities and the slow diffusion process, the calculation time of the current computer program is excessive and constitutes a limitation to its use. This issue could be easily addressed by parallelizing the computation of the solution of the population balance equation. Indeed, the solution of the population balance equation for two different points on the initial bubble density function is currently performed successively on a single microprocessor computer even though they are independent. Therefore, they should be performed in parallel on a multiprocessors computer with as many microprocessors as points taken on the initial bubble density function. This measure will divide the current computational time by the number of microprocessors used.
- Bubble nucleation at the sand grain surface may be significant and should be modeled since oversaturation of the glassmelt with carbon dioxide and oxygen appears to be important. To do so, the density function of unmelted sand grains is needed in order to know the number of nucleation sites. It could be computed by the same method as that presented here for the bubble density function. A different expression for the growth rate $\dot{r}$ will have to be used and is already available in the literature [44,45].
- Nucleation at the refractory walls has been neglected for the sake of simplicity. However, it could be easily accounted for by modeling of heterogeneous nucleation at the refractory walls and by computing the transport of the generated bubbles in a similar manner to that presented above. Finally, the solution is obtained by adding the density functions for bubbles injected from under the batch or from the refractory walls based on the superposition principle.
- It shows that considering the oxygen diffusion in and out of the bubbles has a significant effect on the number and size of bubbles leaving and remaining in the glassmelt. More realistic simulations should include detailed computation of the refining reaction and gas concentrations dissolved in the glassmelt provided that all the thermophysical properties needed be available.

References

[1] L. Pilon, A.G. Fedorov, D. Ramkrishna, R. Viskanta, J. Non-Cryst. Solids, this issue. doi:10.1016/j.jnoncrysol.2004.01.010.
[2] B. Balkanli, A. Ungan, Glass Technol. 37 (4) (1996) 137.
[3] B. Balkanli, A. Ungan, Glass Technol. 3 (5) (1996) 164.
[4] S. Kawachi, Y. Kawase, Glastech. Ber. 71 (4) (1998) 83.
[5] S. Kawachi, Y. Kawase, Glastech. Ber. 71 (5) (1998) 111.
[6] S. Kawachi, Y. Iwatsubo, Glastech. Ber. 72 (7) (1999) 207.
[7] B. Balkanli, A. Ungan, Glass Technol. 37 (3) (1996) 101.

[8] R.G.C Beerkens, H. De Wall, J. Am. Ceram. Soc. 73 (7) (1990) 1857.
[9] M. Cable, J.R. Frade, Glastech. Ber. 60 (11) (1987) 355.
[10] H. Scholze, Glass Nature, Structure and Properties, 3rd Ed., Springer, Berlin, 1991.
[11] L. Pilon, G. Zhao, R. Viskanta, Glass Sci. Technol. 75 (2) (2002) 55.
[12] L. Pilon, PhD thesis, Purdue University, West Lafayette, IN, USA, 2002.
[13] P.R. Laimbock, PhD thesis, Technical University of Eindhoven, Eindhoven, The Netherlands, 1998.
[14] A. Dietzel, Sprechsaal 75 (1942) 82.
[15] N.M. Parikh, J. Am. Ceram. Soc. 41 (1958) 18.
[16] A.G. Fedorov, L. Pilon, J. Non-Cryst. Solids 311 (2002) 154.
[17] S.S. Ghag, P.C. Haves, H.-G. Lee, ISIJ Int. 38 (1998) 1201.
[18] R.H. Doremus, Glass Science, John Wiley, New York, 1994.
[19] N.P. Bansal, R.H. Doremus, Handbook of Glass Properties, Academic, 1986.
[20] R.H. Doremus, J. Am. Ceram. Soc. 43 (1960) 655.
[21] R. Terai, Y. Oishi, Glastech, Ber. 50 (1977) 68.
[22] L. Nemec, M. Mühlbauer, Glastech. Ber. 54 (1981) 99.
[23] M. Cable, Glass Technol. 2 (2) (1961) 60.
[24] S. Kawachi, M. Kato, Glastech. Ber. 72 (6) (1999) 182.
[25] J.E. Shelby, Handbook of Gas Diffusion in Solids and Melts, ASM International, Materials Park, OH, 1996.
[26] L. Pilon, G. Zhao, R. Viskanta, Glass Sci. Technol. 75 (3) (2002) 115.
[27] C. Madivate, F. Müller, W. Wilsmann, J. Am. Ceram. Soc. 81 (1998) 3300.
[28] C. Madivate, J. Am. Ceram. Soc. 81 (1998) 3300.
[29] Y. Zhiqiang, Z. Zhihao, Glastech. Ber. 70 (1997) 165.
[30] J.D. Hoffman, Numerical Methods for Engineers and Scientists, McGraw Hill, New York, 1998.
[31] L. Pilon, R. Viskanta, Int. J. Numer. Meth. Fluid 42 (2003) 1211.
[32] S. Kumar, D. Ramkrishna, Chem. Eng. Sci. 52 (4) (1997) 4659.
[33] D. Ramkrishna, Population Balances, Academic Press, San Diego, CA, 2000.
[34] M. Abramowitz, I.A. Stegun, Handbook of Mathematical Functions, Dover, New York, 1965.
[35] A. Ungan, W.H. Turner, R. Viskanta, Glastech. Ber. 56K (1983) 125.
[36] M. Cable, A.A. Naqvi, Glass Technol. 16 (1) (1975) 2.
[37] M. Cable, C.G. Rasul, J. Am. Ceram. Soc. 50 (10) (1967) 528.
[38] J. Mukerji, A.K. Nandi, K.D. Sharma, Ceram. Bull. 59 (1980) 790.
[39] F. Kramer, Glastech. Ber. 53 (7) (1980) 177.
[40] M.C. Weinberg, P.I.K. Onorato, D.R. Uhlmann, J. Am. Ceram. Soc. 63 (1980) 175.
[41] J.I. Ramos, J. Am. Ceram. Soc. 69 (2) (1986) 149.
[42] H. Akima, ACM Trans. Math. Soft. 4 (2) (1978) 148.
[43] H. Akima, Rocky Mt. J. Math. 14 (1984) 41.
[44] M.K. Choudhary, J. Am. Ceram. Soc. 73 (1990) 3053.
[45] A. Ungan, R.U. Payli, B. Balkanli, J. Am. Ceram. Soc. 77 (7) (1994) 1921.